Available online at www.sciencedirect.com

ScienceDirect

Ceramics International 40 (2014) 2993–3001

CERAMICS INTERNATIONAL

www.elsevier.com/locate/ceramint

Antibacterial responses of zinc oxide structures against *Staphylococcus aureus*, *Pseudomonas aeruginosa* and *Streptococcus pyogenes*

Ling Chuo Ann[a,*], Shahrom Mahmud[a], Siti Khadijah Mohd Bakhori[a], Amna Sirelkhatim[a], Dasmawati Mohamad[b], Habsah Hasan[c], Azman Seeni[d], Rosliza Abdul Rahman[c]

[a]*Nano-optoelectronic Research (NOR) Laboratory, School of Physics, Universiti Sains Malaysia, 11800 Pulau Pinang, Malaysia*
[b]*School of Dental Sciences, Universiti Sains Malaysia, Kubang Kerian, 16150 Kelantan, Malaysia*
[c]*School of Medical Sciences, Universiti Sains Malaysia, Kubang Kerian, 16150 Kelantan, Malaysia*
[d]*Advanced Medical and Dental Institute, Universiti Sains Malaysia, Bertam, 13200 Pulau Pinang, Malaysia*

Received 5 September 2013; accepted 2 October 2013
Available online 10 October 2013

Abstract

The antibacterial responses of zinc oxide (ZnO) structures against *Staphylococcus aureus*, *Pseudomonas aeruginosa*, and *Streptococcus pyogenes* were investigated. Two ZnO powder samples, one with rod-like (ZnO-1) and the other with plate-like (ZnO-2) structures, were characterized for their morphological, structural, and optical properties. The rods were 30–120 nm in diameter, and the plates were 40–100 nm thick. XRD results revealed the wurtzite crystallinity of ZnO with average crystallite sizes of 33.72 (ZnO-1) and 39.25 (ZnO-2) nm. ZnO-2 possessed a relatively higher green photoluminescence than that of ZnO-1, suggesting a relatively higher amount of oxygen vacancies in ZnO-2 structures. Optical density measurements showed that both ZnO samples inhibited the growth of *S. aureus*, *P. aeruginosa*, and *S. pyogenes* by 29–98% after 24 h of treatment. The most dramatic growth inhibition was observed in *S. pyogenes* with 96% and 98% inhibition for ZnO-1 and ZnO-2, respectively, leading to a probable bactericidal phenomenon. The toxicological effect on *S. pyogenes* was probably due to the absence of catalase, making the bacteria vulnerable to the harmful reactive oxygen species (ROS) released by ZnO. ZnO-1 induced higher inhibition toward *S. aureus* and *P. aeruginosa* than that of ZnO-2 because of the smaller particle size of rod structures compared to plate and slab structures. The adhesion of ZnO particles on the membrane of bacteria could be the underlying cause of zinc toxicity effect towards the bacteria. ZnO-1 possessed larger surface area and provided higher amount of zinc atom, thereby inducing higher level of toxicity toward the bacteria. Two possible mechanisms were proposed to explain the inhibition of bacteria, namely, ROS toxicity toward cellular constituents and interaction of zinc with bacteria membrane through adhesion of ZnO particle. Several ZnO morphological-antibacterial correlations were presented in this work.

Keywords: D. ZnO; Antibacterial; ROS; Morphology

1. Introduction

Nanomaterials are gaining considerable interest from various fundamental and applied researchers in the fields of science, engineering, and medicine because of their unique properties and enhanced performance compared with macroscopic materials. The ongoing revolution and upgrading of nanotechnology dramatically affects the development of biomedical and engineering applications. In recent years, nanoparticles smaller than 100 nm in size have been extensively studied because of their wide application in science and technology [1–2].

Zinc oxide (ZnO) is an essential inorganic material with multiple applications in optoelectronics, pigments, cosmetics, pharmaceuticals, varistors, and biosensors [3–9]. ZnO is known to exhibit antimicrobial activity and has higher stability than organic materials. The release of reactive oxygen species (ROS) especially hydrogen peroxide, superoxide anion, hydroxyl radical, and hydroxyl ion [10–11] has been documented as possible mechanisms of the antimicrobial behavior of zinc oxide. With the advancements in nanotechnology, various zinc oxide nanostructures have been prepared, such as rods, plates, tetrapods, tripods, wires, mallets, combs, and flowers [12–16]. The nanosized particles of zinc oxide possess a large surface-to-volume ratio that may exhibit stronger antimicrobial activity. Different structural morphologies of ZnO can exhibit selective antimicrobial

*Corresponding author. Tel.: +60 164708973.
E-mail address: lingchuoann@hotmail.com (L.C. Ann).

0272-8842/$ - see front matter © 2013 Elsevier Ltd and Techna Group S.r.l. All rights reserved.
http://dx.doi.org/10.1016/j.ceramint.2013.10.008

responses. Meanwhile, different bacteria exhibit various affinities toward ZnO structures depending on bioactivity and bacteria life processes. Therefore, further investigation is required to justify the performance of different ZnO structures toward the targeted microbe. The selective bioactivity of bacteria is due to the different biological systems of the bacteria that may render ZnO ineffective for antibacterial application. More studies are necessary to determine the impact of ZnO structures toward various bacteria.

Pathogenic skin bacteria cause many skin infections, including impetigo, folliculitis, furunculosis, carbunculosis, ecthyma, erysipelas, and cellulitis. ZnO is known to cure many kinds of skin diseases and is widely used in health products and cosmetics. Moreover, certain morphological structures of ZnO particularly at the nanoscale are believed to show a relatively greater impact in overcoming skin infections. In this work, three types of pathogenic skin bacteria were studied, namely, *Streptococcus pyogenes*, *Staphylococcus aureus*, and *Pseudomonas aeruginosa*. The effect of ZnO samples that have different structural morphologies on selected skin bacteria was investigated. The level of inhibition of each skin bacteria was also discussed to compare the biological reaction of relevant bacteria with ZnO structures.

2. Experimental details

Two types of ZnO powder were used in this study. Both types were produced via French process described in our previous work [17]. Both samples possessed high purity ($>99.97\%$) and were labeled as ZnO-1 and ZnO-2. The structural morphologies of the both ZnO samples were characterized by field-emission scanning electron microscopy (FESEM; FEI NovaNanoSEM 450) and transmission electron microscopy (TEM; Philips CM12). Electron spectroscopy imaging (ESI) was conducted by energy-filtered transmission electron microscopy (EFTEM; Zeiss Libra 120) to investigate elemental distribution of ZnO particle surfaces. The distribution of zinc atoms and oxygen atoms were localized and are illustrated using different colors (green for Zn; blue for O).

The structural crystallinity of the ZnO powder were investigated using an X-ray diffractometer (model PANalytical X'Pert PRO MED PW3040) with Cu-K_α radiation ($\lambda = 1.5406$ Å) for excitation. The crystallite sizes were calculated from the XRD data and compared with the particle sizes observed from TEM images. Then, ZnO pellets were prepared using a technique introduced in our previous work [17]. The ZnO pellets were characterized for their optical properties using photoluminescence (PL) spectroscopy (Jobin Yvon Horiba HR800UV).

Three types of skin bacteria were chosen in this antibacterial study: two Gram-positive bacteria (*S. pyogenes* ATCC 19615 and *S. aureus* ATCC25923) and one Gram-negative bacteria (*P. aeruginosa* ATCC 27853). Microdilution technique was used to culture and treat the bacteria in a 96-well plate. Initially, bacteria 0.5 Mcfarlands were inoculated and diluted in tryptone soy broth (TSB), producing bacterial colony of about 1×10^6 CFU/ml. Four concentrations of ZnO suspensions were prepared: 1, 2, 3, and 4 mM. 150 µl of adjusted inocula (1×10^6 CFUml) was mixed with 150 µl of ZnO suspension in a 96-well microplate. The final ZnO concentration was halved: 0.5, 1, 1.5, and 2 mM. The mixtures of ZnO and bacteria in TSB were incubated at 37 °C for 24 h.

The growth of bacteria was measured using a spectrophotometer (Versamax microplate reader). Using a light source wavelength of 600 nm, optical density (OD) assessment indicated the level of light scattering caused by the bacteria turbidity. A higher number of bacterial colony in the TSB corresponds to a higher OD reading. OD measurements of *S. aureus* and *P. aeruginosa* were conducted hourly up to 8 h. Given the typically slow growth of *S. pyogenes*, bacterial growth was monitored up to 10 h. The percentage inhibition of bacterial growth was determined from the OD after 24 h of incubation. The antibacterial test was done in triplicate, and the average of three ODs was calculated. A negative control (bacteria and TSB) was also prepared for the measurement.

To observe the morphological structures of the bacteria, a mixture of bacteria and TSB was fixed and processed. The bacteria were washed with phosphate buffer 0.2 M and fixed with McDowell–Trump fixatives. Subsequently, the samples were post-fixed in 1% osmium tetroxide for 1 h, washed with distilled water, dehydrated with ethanol, and treated with hexamethyldisilazane. Lastly, the samples were air dried at room temperature. The dried cells (powder form) were mounted on a FESEM specimen stub with a double-sided carbon tape and coated with platinum. The morphologies of the bacteria were observed under FESEM (FEI).

Numerical data of OD measurements were analyzed for significance using Sigma-plot's *t*-test ($n = 3$). Values are reported as mean ± standard deviation. The threshold for significance was set at $p < 0.05$.

3. Result and discussions

3.1. Morphological and atomic mapping analyses

Figs. 1 and 2 show the morphology and structural details of the two types of ZnO, namely, ZnO-1 and ZnO-2. Fig. 1(a) shows that the morphologies of ZnO-1 are made of several structures: micro/nanorods and irregular-shaped particles. Most structures (about 70%) possess rod-shaped structures. The dimensions of the rods range from 100 nm to 500 nm for the length and from 30 nm to 120 nm for the diameter, respectively. The rod structures are observed to have rounded and tapered tips. The average width sizes were calculated from 100 particles based on many TEM images such as in Fig. 1(b–c). The nanoscale widths have the highest percentage (26%) in the 51–60 nm range [Fig. 1(d)]. The microscopic particles are mostly irregular-shaped particles that are not desired, and their formations were due to the non-uniform crystallization condition during Zn oxidation [17]. Fig. 1(e) shows the elemental mapping of Zn atom and O atom in the ZnO structures using EFTEM (ESI). Results reveal the non-stoichiometric distribution of Zn and O atoms on the surface of ZnO rod structures, whereby the rod structures possess a relatively higher content of O atom on the surface than Zn atom [18].

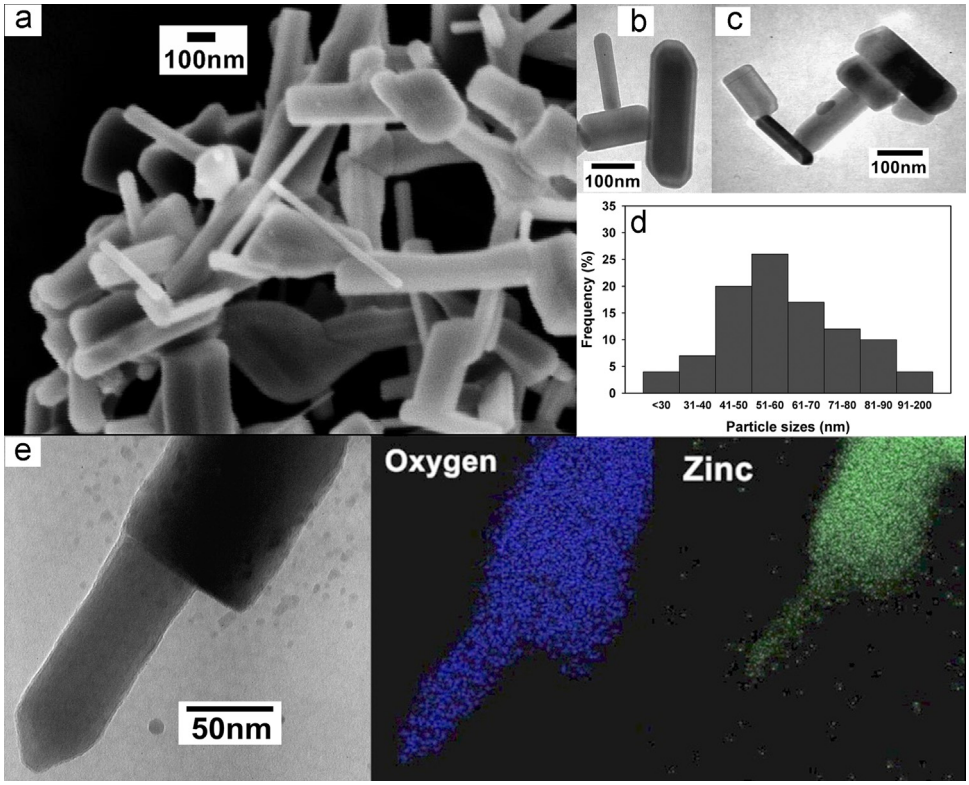

Fig. 1. (a) FESEM micrographs of ZnO-1 powder; (b–c) TEM images of ZnO-1 powder; (d) Percentage frequency of particle sizes based on TEM images; and (e) EFTEM micrographs and ESI elemental mapping. (For interpretation of the references to color in this figure, the reader is referred to the web version of this article.)

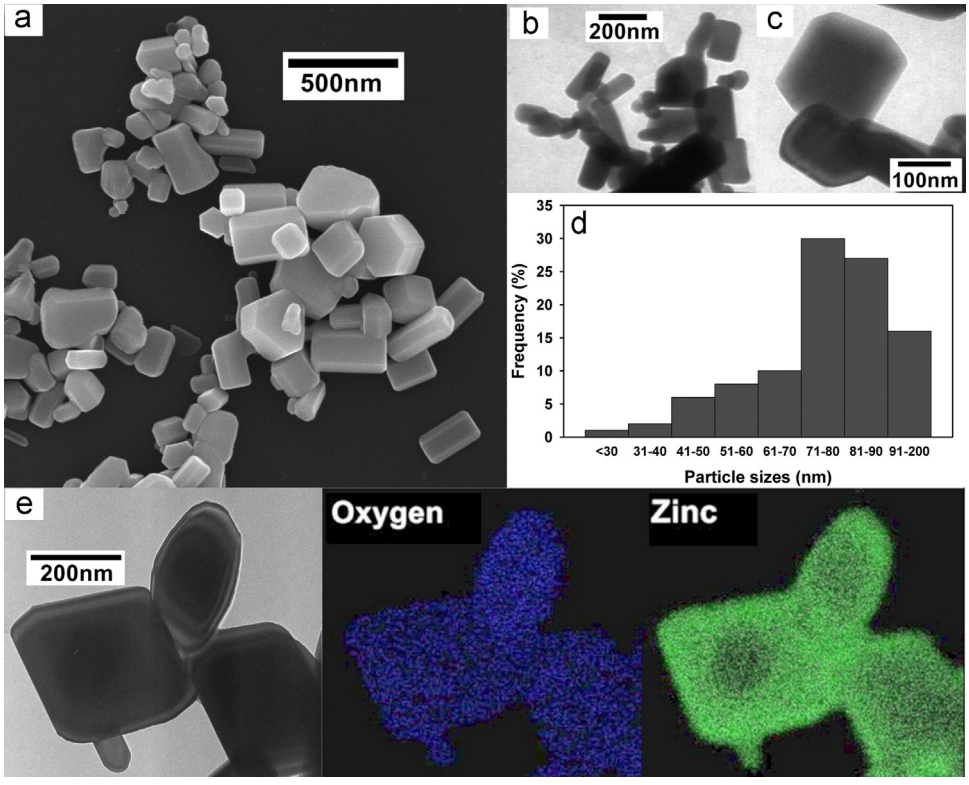

Fig. 2. (a) FESEM micrographs of ZnO-2 powder; (b–c) TEM images of ZnO-2 powder; (d) Percentage frequency of particle sizes based on TEM images; (e) EFTEM micrographs and ESI elemental mapping. (For interpretation of the references to color in this figure, the reader is referred to the web version of this article.)

Fig. 2(a) shows the FESEM image of ZnO-2 that consists of structures resembling plates, slabs, and irregular-shaped particles. The lengths and widths of the plate structures are 120–400 and 40–200 nm, respectively. Based on the average particle sizes calculated from 100 particles from TEM images such as Fig. 2(b–c), the highest percentage of particles sizes (31%) fall within 71–80 nm range [Fig. 2(d)]. Fig. 2(e) exhibits elemental mapping of plate and slab structures on ZnO-2. The concentration of oxygen atoms is evidently less than that of zinc atoms on the particle surface. Comparing the ESI elemental mapping of both ZnO-1 and ZnO-2 samples, the atomic ratio of oxygen to zinc (O:Zn) of ZnO-1 structures is observed to be higher than that of ZnO-2. The different morphologies of ZnO structures exhibit different O:Zn ratios on the particle surface [18].

3.2. Structural and optical properties

The X-ray diffraction (XRD) spectra of ZnO-1 and ZnO-2 are shown in Fig. 3(a). The XRD reflections can be indexed to the international crystallographic data table JCPDS Card no. 800074, which have lattice constants of $a=3.254$ Å and $c=5.215$ Å. Both samples exhibit a wurtzite polycrystalline nature of pure ZnO having no diffraction lines associated with impurities detected. The sharp reflection peaks indicate good crystallinity of both samples. Their preferential orientations are composed of (101), (100), (002), (110), (103), and (102) planes. Based on the three dominant peaks (101), (100), and (002), the average lattice spacing d of ZnO-1 and ZnO-2 are calculated from Bragg's equation:

$$d = \frac{n\lambda}{2 \sin \theta} \quad (1)$$

where λ (1.5406 Å) is the X-ray wavelength, and θ is the diffraction angle. The magnitude of lattice spacing of ZnO-1 and ZnO-2 are 2.4800 and 2.4788 nm, respectively. ZnO-1 is found to have lattice spacing comparable to that of ZnO-2.

The particle size of each sample was estimated from the X-ray line-broadening method using the Debye–Scherer formula [19]:

$$t = \frac{0.9\lambda}{FWHM \cos \theta} \quad (2)$$

where t is the particle size in nanometers, λ is the wavelength of radiation (1.5406 Å), FWHM is the peak width at half-maximum intensity, and θ is the peak position. The (101), (100), and (002) planes were used to calculate the crystallite size, and the results are presented in Table 1. The average particle sizes of ZnO-1 and ZnO-2 are 33.72 and 39.25 nm, respectively. The calculated particle sizes are consistent with the results measured by TEM images [Figs. 1(d) and 2(d)]. Given the wide range of particles sizes of ZnO-1 and ZnO-2, the TEM images provided better results of particle size measurement than XRD calculation.

Fig. 3(b) shows the room temperature PL spectra of ZnO-1 and ZnO-2. Both samples present dominant UV emissions and weak green emissions. The intense near-band-edge (NBE) emission is located at 375 (ZnO-1) and 378 (ZnO-2) nm, corresponding to the optical bandgap 3.31 (ZnO-1) and 3.29 (ZnO-2) eV, respectively. The sharp NBE absorption reveals the high purity and crystalline structure of ZnO. The obtained optical bandgaps are slightly smaller than that of ZnO bulk ($E_g=3.37$ eV). This finding is probably due to defects particularly oxygen vacancies and zinc interstitials [20], which may reduce the optical bandgap of ZnO samples. Other factors such as polaron, strain, grain boundary, and crystal imperfections [21] can cause this phenomenon to exist.

A broad visible emission is observed from 450 nm until 700 nm (from blue to red emission). The origin of the visible emission remains debatable and is generally attributed to deep-level defects such as oxygen vacancies, zinc vacancies and oxygen interstitials serving as a recombination centers. The highest intensity of visible light is green emission (546 nm), which is attributed to single ionized (V_o^+) and doubly ionized (V_o^{++}) oxygen vacancy [22,23]. The inset of Fig. 3(b) shows that the intensity of the visible emission of ZnO-1 (4.2×10^3 a.u.) is lower than that of ZnO-2 (1.5×10^4 a.u.). This phenomenon indicates the relatively lower amount of oxygen vacancies on the ZnO-1 surface than on the ZnO-2 surface. This observation well agrees with the ESI elemental mapping results that reveal a higher O:Zn ratio on the rod structure surface but lower O:Zn ratio on plates and slabs surfaces. Consequently, ZnO-1 tends to have relatively higher O:Zn ratio than ZnO-2. Table 1 summarizes the PL emission of ZnO-1 and ZnO-2.

3.3. Antibacterial properties

3.3.1. S. aureus

Fig. 4 shows the antibacterial test of ZnO-1 and ZnO-2 against *S. aureus*, a round-shaped Gram-positive bacterium. The FESEM

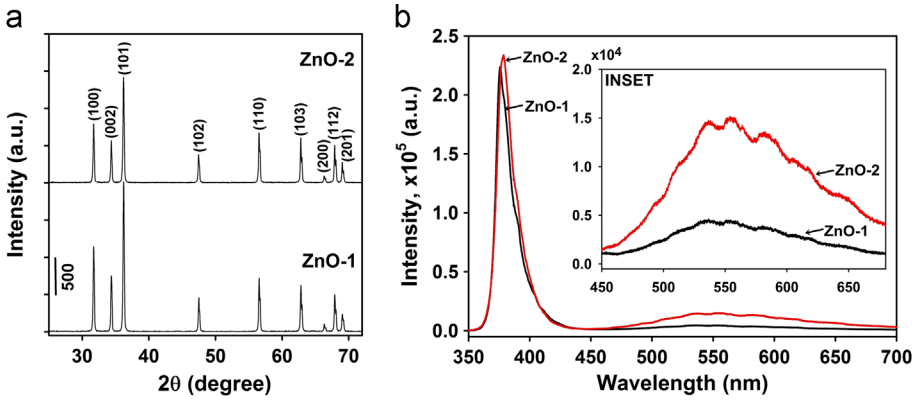

Fig. 3. (a) XRD spectra and (b) PL spectra of ZnO-1 and ZnO-2.

Table 1
Structural parameters and PL emissions of ZnO-1 and ZnO-2.

Samples	Peak position of (101) (deg)	Lattice spacing, d (nm)	Crystallite size, t (nm)	PL peak (nm)	Energy bandgap (eV)	Green emission intensity (a.u.)
ZnO-1	36.2220	2.4800	33.72	375	3.31	4.2×10^3
ZnO-2	36.2399	2.4788	39.25	378	3.29	1.5×10^4

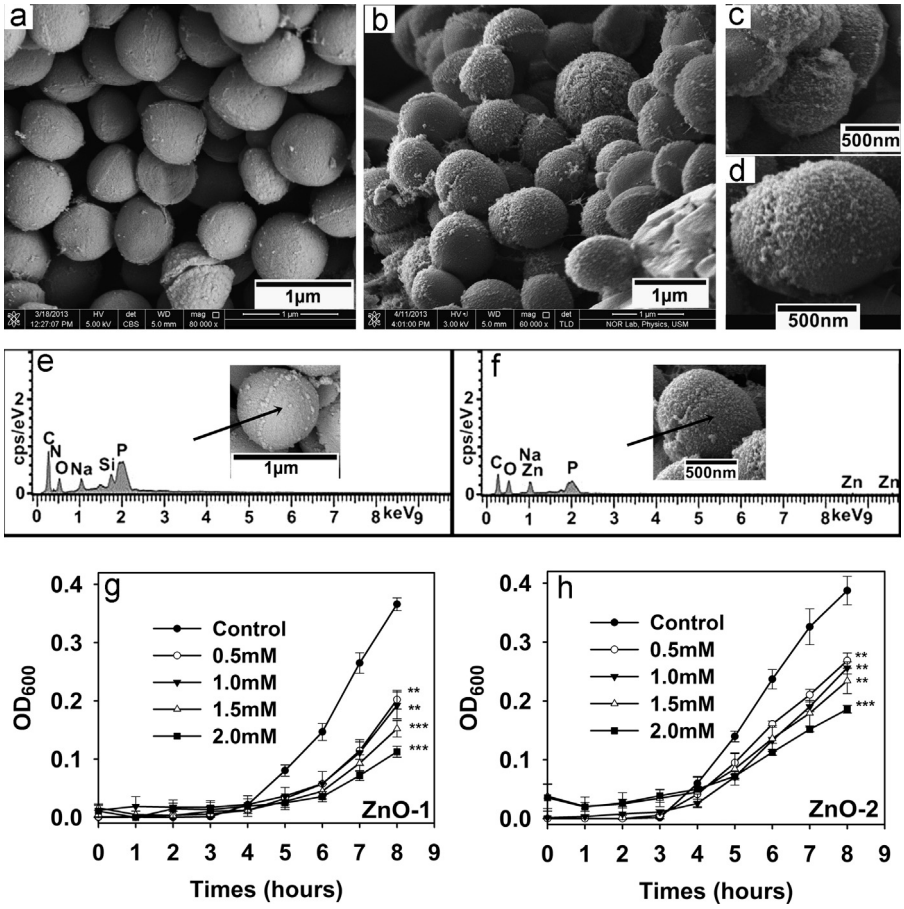

Fig. 4. FESEM micrographs of *S. aureus* (a) without treatment and (b–d) treated with ZnO-2; EDS spectra of *S. aureus* (e) without treatment and (f) treated with ZnO-2; OD measurement of *S. aureus* growth being treated with (g) ZnO-1 and (h) ZnO-2. Plots represent average OD ± SD ($n=3$, $^{**}p<0.01$, $^{***}p<0.001$).

images reveal the morphology of the *S. aureus* control [Fig. 4(a)] and treated *S. aureus* [Fig. 4(b–d)]. The size of *S. areus* appears to be 0.7–0.9 μm, with an average of 0.8 μm. Under ZnO treatment, the surface of the bacteria is covered with ZnO particles. This finding is verified by the EDS measurement (using a spot scan) conducted on the surface of untreated *S. aureus* [Fig. 4(e)] and treated *S. aureus* [Fig. 4(f)]. Zn atom was detected on treated *S. aureus*, but Zn atom was absent on the surface of the untreated *S. aureus*. Results show that the ZnO particles were largely attached and perhaps reacted with the membrane surface of *S. aureus*. ZnO samples potentially inhibit the growth of *S. aureus* through direct contact with the cell membrane.

Fig. 4(g) and (h) shows the OD measurements of *S. aureus* treated with ZnO-1 and ZnO-2, respectively. *S. aureus* exhibited exponential growth in TSB medium, in which it rapidly grew after 5–8 h of incubation. Both samples have similar inhibition trends in that increased ZnO concentration (0.5, 1.0, 1.5, and 2.0 mM) enhanced the inhibition of *S. aureus*. Compared with the *S. aureus* control, the OD remarkably decreased when ZnO samples were added. Using a concentration of 2 mM, ZnO-1 reduces the OD from 0.366 ± 0.021 to 0.112 ± 0.009; whereas ZnO-2 reduces the OD from 0.387 ± 0.024 to 0.186 ± 0.006. Both ZnO (0.5, 1.0, 1.5 and 2.0 mM) samples significantly lower the bacterial growth ($n=3$, $p<0.01$). After 8 h of ZnO treatment, the amount of bacterial cells decreased by 69% (ZnO-1) and 52% (ZnO-2) compared with the bacteria control.

3.3.2. *P. aeruginosa*

P. aeruginosa is a rod-shaped Gram-negative bacterium of about 0.4 μm in diameter and 1.2 μm long. Fig. 5(a) shows the *P. aeruginosa* control, and Fig. 5(b–d) shows *P. aeruginosa* treated with ZnO. The bacteria are found to have some rupture and damage on the membrane surface resulting from the

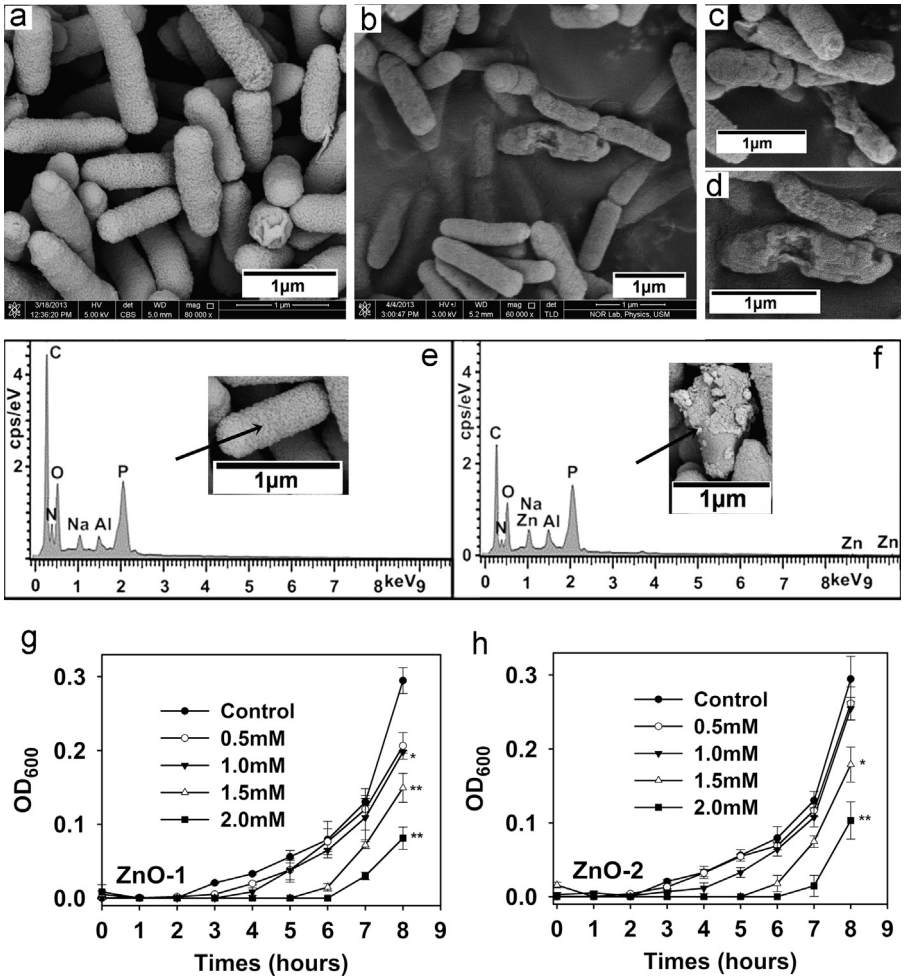

Fig. 5. FESEM micrographs of *P. aeruginosa* (a) without treatment and (b–d) treated with ZnO-1; EDS spectra of *P. aeruginosa* (e) without treatment and (f) treated with ZnO-1; OD measurement of *P. aeruginosa* growth being treated with (g) ZnO-1 and (h) ZnO-2. Plots represent average OD ± SD ($n=3$, $^{*}p<0.05$, $^{**}p<0.01$).

toxicity of ZnO towards the bacteria. The "shrinkage" of the bacteria [Fig. 5(c–d)] revealed bacteria-static effect of ZnO against *P. aeruginosa*. EDS measurement [Fig. 5(e–f)] verified the presence of ZnO on the bacterial surface. The attachment of ZnO particles onto the surface membrane of *P. aeruginosa* induced toxicity toward the bacterial cell and this might resulted in the membrane damage of some of the bacteria population.

Fig. 5(g–h) illustrates the OD measurements of *P. aeruginosa* growth. The bacteria rapidly grew and reproduced after 4 h of incubation. Increased concentration of ZnO-1 and ZnO-2 resulted in decreased OD of *P. aeruginosa* and lowered the growth of bacteria. Using a concentration of 2 mM, ZnO-1 reduced OD from 0.294 ± 0.018 (control) to 0.081 ± 0.025; whereas ZnO-2 reduced the OD from 0.294 ± 0.061 (control) to 0.101 ± 0.035. ZnO-1 significantly decreased the bacterial growth at concentration more than 1.0 mM ($n=3$, $p<0.05$); whereas ZnO-2 significantly inhibited the bacteria growth at concentration higher than 1.5 mM ($n=3$, $p<0.05$). After 8 h of treatment, ZnO-1 and ZnO-2 reduced the amount of *P. aeruginosa* by 72% and 66%, respectively. Both ZnO samples potentially slowed down the growth and also partially killed *P. aeruginosa*.

3.3.3. *S. pyogenes*

ZnO samples were also used to examine the antibacterial response against *S. pyogenes*, a spherical and Gram-positive bacterium. Different from *S. aureus*, *S. pyogenes* is catalase negative. Therefore, it is worthy to study the effect of ZnO samples on catalase-negative bacteria that may have different interactions and responses to ZnO particles. Fig. 6(a) shows that the diameter of *S. pyogenes* is about 0.7 μm. Under ZnO treatment [Fig. 6(b)], *S. pyogenes* bacteria were largely destroyed and killed. EDS measurement [Fig. 6(c–d)] revealed the presence of ZnO particles on the treated bacteria and there were no ZnO traced in the untreated bacteria.

S. pyogenes showed rapid growth after 6 h of incubation, as illustrated in Fig. 5(e–f). Bacterial growth is slower than that of *S. aureus* and *P. aeruginosa*. Therefore, OD measurements were conducted until 10 h to justify the consistency of bacterial growth. With a concentration of 0.5 mM, both ZnO-1 and ZnO-2 showed high inhibition toward *S. pyogenes*. After 10 h of incubation, the ODs of bacteria treated with ZnO-1 and ZnO-2 decreased from 0.479 ± 0.010 to 0.078 ± 0.004 and from 0.478 ± 0.008 to 0.075 ± 0.001, respectively. Reduction in bacterial amount of ZnO-1 and ZnO-2 were 84% and 85%,

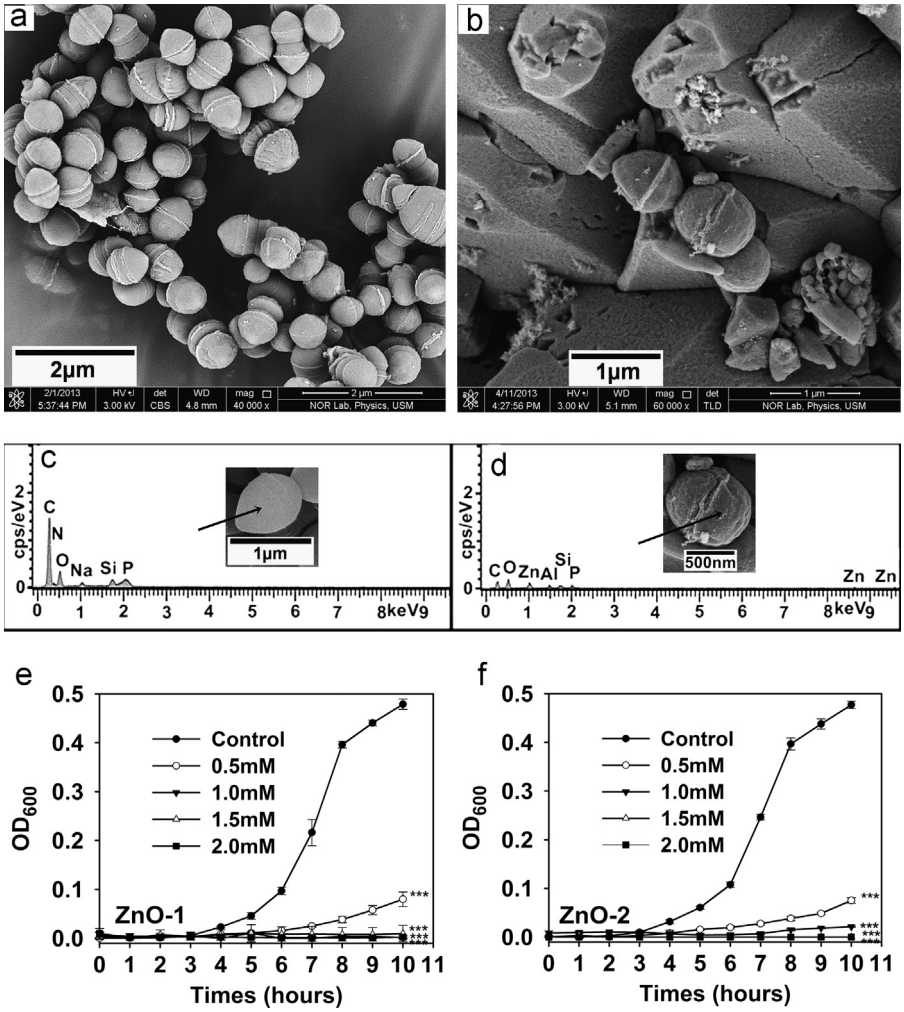

Fig. 6. FESEM micrographs of *S. pyogenes* (a) without treatment and (b–d) treated with ZnO-2; EDS spectra of *S. pyogenes* (e) without treatment and (f) treated with ZnO-2; OD measurement of *S. pyogenes* growth being treated with (g) ZnO-1 and (h) ZnO-2. Plots represent average OD ± SD ($n=3$, $^{***}p<0.001$).

respectively. Concentrations of 1.0, 1.5, and 2.0 mM suppressed the growth of *S. pyogenes* and caused a high percentage of bacterial inhibition of $>95\%$. ZnO (>0.5 mM) significantly inhibited the bacteria growth ($n=3$, $p<0.001$). ZnO-1 and ZnO-2 are believed to exert high toxicity effect and potential bactericidal effect toward the bacteria. After 8–10 h of incubation, ZnO-1 and ZnO-2 exhibited the greatest affinity toward *S. pyogenes* compared with *S. aureus* and *P. aeruginosa*.

3.4. Probable antibacterial mechanisms

The exact mechanism of the antibacterial action of microscale and nanoscale ZnO particles has not been conclusive. Considering the responses of different bacteria species to ZnO-1 and ZnO-2 samples, the mechanism of antibacterial behavior depends on the bacteria type and ZnO properties. The inhibition percentage of *S. aureus*, *P. aeruginosa*, and *S. pyogenes* after 24 h of treatment was determined from the OD measurement and calculated based on the bacterial control from the equation:

$$\text{Percentage inhibition} = \left(1 - \frac{\text{OD}_{\text{viable cell}}}{\text{OD}_{\text{bacteria control}}}\right) \times 100\% \qquad (3)$$

Fig. 7 shows the percentage inhibition of bacteria by 2 mM ZnO-1 and ZnO-2. Three types of bacteria exhibited different inhibition responses after treatment with ZnO structures for 24 h.

After 24 h of treatment, ZnO-1 and ZnO-2 inhibited *S. aureus* growth by $36 \pm 3\%$ and $29 \pm 2\%$, respectively. The toxicity effect of ZnO structures towards *S. aureus* was the lowest among the three bacteria in the current study. It is known that *S. aureus* tends to develop defenses against oxidative stress by releasing responsive gene products such as superoxide dismutase, catalase, and thioredoxin reductase. Superoxide dismutase may convert O_2^- to H_2O_2, catalase may convert H_2O_2 to H_2O and O_2, and thioredoxin reductase may protect cell against toxic oxygen species [24–26]. Therefore, *S. aureus* could build an effective "shield" to reduce the toxicity of the ZnO samples. However, some ZnO particles are observed to be attached onto the surface membrane of the bacteria, as shown in Fig. 4(b–d). The EDS result [Fig. 4(f)] also showed the presence of ZnO particles on the bacterial surface. The antibacterial action of *S. aureus* was possibly due to the damage inflicted to the membrane cell wall by the adhesion of ZnO particles onto the cell membrane. Therefore, this mechanical damage could be another probable inhibition

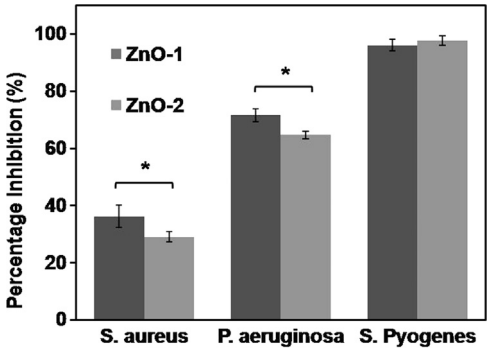

Fig. 7. Percentage inhibition of S. aureus, *P. aeruginosa* and *S. pyogenes* being treated with 2 mM of ZnO-1 and ZnO-2. Plots represent mean ± SD ($n=3$, $^{*}p<0.05$).

mechanism on *S. aureus*. This mechanism was also proposed by Stoimenov et al. [27].

Meanwhile, ZnO-1 and ZnO-2 reduced *P. aeruginosa* growth by 72 ± 2% and 65 ± 1%, respectively. *P. aeruginosa* has a Gram-negative cell wall composed of an outer membrane, a thin peptidoglycan, and a plasma membrane. The cell wall has a relatively thinner peptidoglycan layer than gram-positive bacteria (*S. aureus* and *S. pyogenes*) [28]. Consequently, the wall of *P. aeruginosa* would be less resistant to osmotic pressure. The attachment of ZnO onto the membrane might affect cell wall function and may disrupt the membrane system. Cell membrane rupture of *P. aeruginosa* can be observed in the FESEM image [Fig. 5(b–d)]. Localized physical damage to the membrane cell wall by particle adhesion was more evident on *P. aeruginosa* than on *S. aurues*, probably because of the thinner peptidoglycan structure of *P. aeruginosa* membrane. Oxidative stress potentially disrupted the bacterial cell wall and induced toxicological impact toward the cell.

Comparison of the results of antibacterial capability of ZnO-1 and ZnO-2 revealed that ZnO-1 had a higher inhibition percentage of *S. aureus* ($p<0.05$) and *P. aeruginosa* ($p<0.05$) than ZnO-2. This finding was due to the different particle sizes of the two samples [TEM images in Figs. 1(b–d) and 2(b–d)], where ZnO-1 contained more nanorod structures whereas ZnO-2 had more microplate structures. Rods had larger surface-to-volume ratio than plates/slabs, thereby contained higher amount of zinc and oxygen atoms on the surface. A higher zinc content can caused relatively higher toxicity towards bacteria when the nanorod attached and reacted with the membrane of the bacteria.

From Fig. 7, ZnO-1 and ZnO-2 caused the greatest inhibition toward *S. pyogenes*, i.e., 96 ± 2% and 98 ± 1%, respectively. The high percentage of inhibition can be considered as a bactericidal effect on the bacteria. The FESEM image [Fig. 6(b)] and OD measurement [Fig. 6(e–f)] also showed consistent results, wherein *S. pyogenes* were mostly disrupted when ZnO-1 and ZnO-2 came in contact with the bacteria. The antibacterial activity in this instance was presumably due to the production of ROS, such as hydrogen peroxide (H_2O_2), superoxide anion (O_2^-), and hydroxyl radicals ($OH\cdot$). These ROS were toxic to the cells as they could damage cellular constituents such as DNA, lipids, and protein [29–31]. Furthermore, the different amounts of oxygen atoms on the ZnO structures are another possible contribution to the ROS production rate. ZnO-1 possessed many rod structures rich with oxygen atom [ESI image in Fig. 1(e)]; whereas ZnO-2 contained many plate structures deficient in oxygen atom [ESI image in Fig. 2(e)]. The PL results [Fig. 3(b)] also showed a higher amount of oxygen vacancies/defects on the ZnO-2 structure than that of ZnO-1 structure. Higher amount of oxygen atoms on rod surface is believed to induce higher level of ROS in the mixture resulting in intense oxidative stress towards the bacteria. *S. pyogenes* is known as catalase-negative bacteria. Compared to *S. aureus*, *S. pyogenes* does not produce any catalase that can neutralize the ROS effect and protect the cell from the ROS toxicity. Therefore, *S. pyogenes* could be exposed to ROS toxicological interaction induced by ZnO particles. Eventually, the bacteria were severely damaged within several hours of incubation. The concentrations of ZnO-1 and ZnO-2 that could lead to the bactericidal effect toward *S. pyogenes* were observed to be above 0.5 mM, as shown in the OD measurement [Fig. 6(e–f)].

Two mechanisms are proposed for the inhibition of bacterial growth: zinc toxicity of cell membrane by adhesion of ZnO particles, and ROS toxicity toward bacteria constituents. Different strains of bacteria may possess different responses to the ZnO particles. Therefore, the effect of ZnO structures toward the other strains of bacteria need to be elucidated in future works.

4. Conclusions

ZnO-1 and ZnO-2 showed a remarkable antibacterial activity towards *S. pyogenes*. This phenomenon was due to the toxicity effect of ROS that could kill effectively kill *S. pyogenes*. Interesting ZnO morphological-antibacterial correlation was discussed. The rod structures of ZnO-1 caused higher antibacterial response towards *S. aureus* and *P. aeruginosa* compared to plate/slab structures of ZnO-2. Smaller particles size of rod structures provided relatively greater surface area and higher amount of zinc atoms that triggered toxicity effect towards the bacteria. The adhesion of ZnO structures on the *S. aureus* and *P. aeruginosa* had induced physical damage to the membrane of the bacteria cells.

Acknowledgments

This work was supported by Universiti Sains Malaysia through a Research University (Individual) Grant (1001/PFIZIK/814174). We acknowledge assistance from Microbiology Lab and NOR Lab.

References

[1] D. Sharma, J. Rajput, B.S. Kaith, M. Kaur, S. Sharma, Synthesis of ZnO nanoparticles and study of their antibacterial and antifungal properties, Thin solid films 519 (2010) 1224–1229.

[2] N. Iqbal, M.R.A. Kadir, N.A.N.N. Malek, N.H. Mahmood, M.R. Murali, T. Kamarul, Rapid microwave assisted synthesis and characterization of nanosized silver-doped hydroxyapatite with antibacterial properties, Materials Letters 89 (2012) 118–122.
[3] A. George, S.K. Sharma, S. Chawla, M.M. Malik, M.S. Qureshi, Detailed of X-ray diffraction and photoluminescence studies of Ce doped ZnO nanocrystals, Journal of Alloys and Compounds 509 (2011) 5942–5946.
[4] S.F. Yu, Y. Clement, S.P. Lau, Y.G. Wang, H.W. Lee, B.K. Tay, Ultraviolet amplified spontaneous emission from zinc oxide ridge waveguides on silicon substrate, Applied Physics Letters 83 (2003) 4288–4290.
[5] S. Ekambaram, Solution combustion synthesis and luminescent properties of perovskite red phosphors with higher CRI and greater lumen output, Journal of Alloys and Compounds 390 (2005) L4–L6.
[6] R.P. Sheldon, F.P. David, G.P. Robert, A.M. Mark, K. Nikiforos, Microfine zinc oxide is a superior sunscreen ingredient to microfine titanium dioxide, Dermatologic Surgery 26 (2000) 309–314.
[7] S. Baldwin, M.R. Odio, S.L. Haines, R.J. Oconnor, J.S. Englehart, A. T. Lane, Skin benefits from continuous topical administration of a zinc oxide/petrolatum formulation by a novel disposable diaper, Journal of the European Academy of Dermatology and Venereology 15 (2001) 5–11.
[8] M.L. Hans, A.M. Lowman, Biodegradable nanoparticles for drug delivery and targeting, Current Opinion in Solid State and Materials Science 6 (2002) 319.
[9] S. Krishnamoorthy, T. Bei, E. Zoumakis, G.P. Chrousos, A.A. Iliadis, Morphological and binding properties of interleukin-6 on thin ZnO films grown on (100) silicon substrates for biosensor applications, Biosensors and Bioelectronics 22 (2006) 707–714.
[10] O. Yamamoto, Influence of particle size on the antibacterial activity of zinc oxide, International Journal of Inorganic Materials 3 (2001) 643–646.
[11] J. Sawai, Quantitative evaluation of antibacterial activities of metallic oxide powders (ZnO, MgO and CaO) by conductimetric assay, Journal of Microbiological Methods 54 (2003) 177–182.
[12] S. Mahmud, M.J. Abdullah, G.A. Putrus, J. Chong, A.K. Mohamad, Nanostructure of ZnO fabricated via French process and its correlation to electrical properties of semiconducting varistors, Synthesis and Reactivity in Inorganic, Metal-Organic, and Nano-Metal Chemistry 36 (2006) 155–159.
[13] S. Mahmud, M.J. Abdullah, M.Z. Zakaria, Growth model for nanoplates and nanoboxes of zinc oxide from a catalyst-free combust-oxidized process, Synthesis and Reactivity in Inorganic, Metal-Organic, and Nano-Metal Chemistry 36 (2006) 17–22.
[14] S. Mahmud, M.J. Abdullah, J. Chong, A.K. Mohamad, M.Z. Zakaria, Growth model for nanomallets of zinc oxide from a catalyst-free combust-oxidised process, Journal of Crystal Growth 287 (2006) 118–123.
[15] J.S. Tawale, K.K. Dey, R. Pasricha, K.N. Sood, A.K. Srivastava, Synthesis and characterization of ZnO tetrapods for optical and anti-bacterial applications, Thin Solid Films 519 (2010) 1244–1247.
[16] Z.L. Wang, Nanostructures of zinc oxide, Materials Today 7 (2004) 26–33.
[17] S. Mahmud, One-dimensional growth of zinc oxide nanostructures from large micro-particles in a highly rapid synthesis, Journal of Alloys and Compounds 509 (2011) 4035–4040.
[18] L.C. Ann, S. Mahmud, S.K.M. Bakhori, Electron spectroscopy imaging and surface defect configuration of zinc oxide nanostructures under different annealing ambient, Applied Surface Science 265 (2013) 137–144.
[19] B.D. Cullity, in: Elements of X-ray Diffraction, Addition-Wesley, Reading, MA, 1978.
[20] H. Kind, H. Yan, M. Law, B. Messer, P. Yang, Nanowire Ultraviolet Photodetectors and Optical Switches, Advanced Materials 14 (2002) 158–160.
[21] R.G. Singh, F. Singh, V. Kumar, R.M. Mehra, Growth kinetics of ZnO nanocrystallites: structural, optical and photoluminescence properties tuned by thermal annealing, Current Applied Physics 11 (2011) 624–630.
[22] Y.W. Heo, D.P. Norton, S.J. Pearton, Origin of green luminescence in ZnO thin film grown by molecular-beam epitaxy, Journal of Applied Physics 98 (2005) 073502.
[23] A.V. Dijken, E.A. Meulenkamp, D. Vanmaekelbergh, A. Meijerink, The kinetics of the radiative and nonradiative processes in nanocrystalline ZnO particles upon photoexcitation. Journal of Physical Chemistry B, 104 (2000) 1715.
[24] K.R. Raghupathi, R.T. Koodali, A.C. Manna, Size-dependent bacterial growth inhibition and mechanism of antibacterial activity of zinc oxide nanoparticles, Langmuir 27 (2011) 4020–4028.
[25] A. Ballal, A.C. Manna, Control of thioredoxin reductase gene (trxB) transcription by SarA in Staphylococcus aureus, Journal of Bacteriology 192 (2010) 336–345.
[26] J.S. Miller, J.M. Quarles, Cytometry, Flow cytometric identification of microorganisms by dual staining with FITC and PI 11 (1990) 667–675.
[27] P.K. Stoimenov, L.K. Rosalyn, L.K. George, Metal oxide nanoparticles as bactericidal agents, Langmuir 18 (2002) 6679.
[28] J.M. Willey, L.M. Sherwood, C.J. Woolverton, Prescott's Microbiology. 2011, New York: Mc Graw Hill.
[29] G. Storz, J.A. Imlay, Oxidative stress, Clinics in Occupational and Environmental MedicineCurrent Opinion in Microbiology 2 (1999) 188–194.
[30] I.G. Kirkinezos, C.T. Moraes, Reactive oxygen species and mitochondrial diseases, Seminar in Cell and Development Biology 12 (2001) 449–457.
[31] T. Xia, M. Kovochich, A. Nel, The role of reactive oxygen species and oxidative stress in mediating particulate matter injury, Clinics in Occupational and Environmental Medicine 5 (2006) 817–836.